A Letters Journal Exploring the Frontiers of Physics

January 2015

EPL, **109** (2015) 17001
doi: 10.1209/0295-5075/109/17001

www.epljournal.org

Femtosecond-laser–induced modifications in Co/Pt multilayers studied with tabletop resonant magnetic scattering

C. Weier[1], R. Adam[1], D. Rudolf[1], R. Frömter[2], P. Grychtol[3], G. Winkler[2], A. Kobs[2], H. P. Oepen[2], H. C. Kapteyn[3], M. M. Murnane[3] and C. M. Schneider[1]

[1] *Forschungszentrum Jülich GmbH, Peter Grünberg Institut (PGI-6), JARA-FIT - 52425 Jülich, Germany*
[2] *Universität Hamburg, Institut für Angewandte Physik - Jungiusstr. 11, 20355 Hamburg, Germany*
[3] *University of Colorado, Department of Physics and JILA - Boulder, CO 80309, USA*

received 11 July 2014; accepted in final form 16 December 2014
published online 14 January 2015

PACS 75.70.Kw – Domain structure (including magnetic bubbles and vortices)
PACS 61.05.cf – X-ray scattering (including small-angle scattering)

Abstract – We characterize the magnetic domain structure of Co/Pt multilayer films on length scales below one hundred nanometers using resonant magnetic scattering and magnetic force microscopy. The extreme ultraviolet light for the scattering experiment is created by a laser-based high-order harmonic generation source. After illumination with intense ultrashort infrared laser pulses, we observe pronounced changes in the magnetic structure and morphology. This study points out the importance of a detailed analysis of the different laser-induced modifications of a magnetic thin film that influence the scattering patterns.

A detailed understanding of the static and dynamic behavior of magnetic domains is essential for both fundamental research and for applications in spin electronics. Exploring magnetic structures, especially magnetic domain dynamics on nanometer length scales with femtosecond temporal resolution is particularly interesting. However, such studies require an ultrashort-pulse light source with a short wavelength and a sufficient photon flux. Very recently, ultrashort synchrotron X-ray pulses produced by femtosecond slicing [1,2], free-electron lasers [3] and tabletop high-order harmonic generation (HHG) light sources [4–7] opened the door for such dynamical studies with the additional benefit of element selectivity. To date, only a few experiments have been able to resolve magnetic domain dynamics both temporally and spatially, with femtosecond and nanometer precision [3,8–10]. While large-scale synchrotrons and free-electron lasers can produce X-rays with a high radiant power, laser-based tabletop HHG sources have demonstrated an increasing ability of generating fully coherent short wavelength radiation up to the soft X-ray region of the electromagnetic spectrum with pulse durations in the femtosecond-to-attosecond regime [11]. Moreover, phase matching of circularly polarized high harmonics has recently been demonstrated, which are bright enough for measurements of X-ray magnetic circular dichroism [12]. Furthermore, HHG sources have been used in a variety of imaging experiments, using zone plates [13] and lensless coherent imaging [14,15], thereby paving the way for element-specific investigations of magnetic phenomena on their fundamental time and length scales.

In this work we employ resonant magnetic scattering (RMS) driven by a HHG source to map the magnetic domain pattern in reciprocal space. Co/Pt multilayer films are studied before and after illumination with intense ultrashort infrared laser pulses. We analyze the impact of this exposure on the magnetic domain pattern, as well as on the sample morphology, employing magnetic force microscopy (MFM) and we compare our findings with the observed RMS patterns. Moreover, we show that the laser-illumination causes permanent as well as reversible modifications of the domain structure.

The interaction between 3d ferromagnets and photons with energies corresponding to the $M_{2,3}$-absorption edges, *i.e.*, 53 eV (Fe), 60 eV (Co) and 68 eV (Ni), results in a resonant enhancement of the magneto-optical effects, enabling studies of magnetic properties with element selectivity [16,17]. In resonant scattering experiments using either XUV light or X-rays, both the sample morphology and the magnetic domains contribute to the measured signal. The magnetic contrast originates from magnetic circular dichroism, which is sensitive for the magnetization component in beam direction, *i.e.*, perpendicular to the sample plane [18–20].

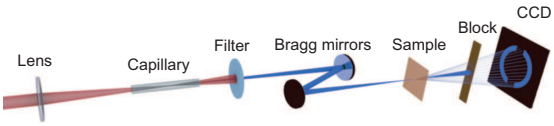

Fig. 1: (Colour on-line) Schematics of the RMS experiment using a laser-driven HHG source. Intense laser pulses are focused into a neon-filled capillary, generating XUV light. A filter removes the laser radiation, while the HHG beam is further monochromatized and focused onto the sample. The scattered light is measured with a CCD camera and the transmitted beam is blocked by a metallic wire.

Figure 1 shows the schematics of the experimental setup. XUV light is generated by focusing ultrashort laser pulses (Dragon laser amplifier, KMLabs, 2 mJ per pulse, 3 kHz, pulse width 35 fs, central wavelength 780 nm) into a glass capillary filled with neon gas [21]. The laser-generated XUV radiation (43–72 eV) is then separated from the laser light by two 150 nm thin aluminum filters. Due to the high absorption of the XUV radiation in air, all components after the capillary are mounted inside vacuum chambers that are evacuated to 10^{-5} mbar. The XUV beam is reflected from a pair of Bragg mirrors (Mo/Si multilayers) that serve as monochromators to select the 39th harmonic order (62 eV), which is within the $M_{2,3}$-absorption edge of Co [22]. The first Bragg mirror, curved with a radius of 1 m, focuses the beam to a spot of approximately 50 μm in diameter at the sample plane. After passing through the sample, the transmitted beam is blocked by a metallic wire, while the scattered XUV light is recorded by a charge coupled device (CCD) camera (Andor iKon-L, 2048 × 2048 array of 13.5 × 13.5 μm^2 pixels).

We investigate magnetron sputtered Pt(5 nm)/$[$Co(0.8 nm)/Pt(1.2 nm)$]_8$/Pt(1.6 nm) multilayer films, which exhibit a canted easy axis of magnetization [23,24]. The substrate is a 50 nm thick Si_3N_4-membrane, supported by a Si frame. Figures 2(a) and (b) show the surface morphology obtained by atomic force microscopy (AFM) and the magnetic domain structure measured with MFM for an as-grown sample (B1). This specimen reveals a maze-like domain pattern for the out-of-plane component of magnetization with an average domain size of about 100 nm. It has been demonstrated that the magnetic properties, including the domain size, of Co/Pt multilayer films can be modified by the implantation of Ga ions [25,26]. In addition, the influence of intense XUV pulses on the magnetic domain structure and on the resonant scattering mechanism has been studied thoroughly using free-electron lasers [20,27,28]. In the here presented study we analyze alterations of the domain pattern induced by infrared laser pulses. Figures 2(c) and (d) show AFM and MFM images for a sample (B2) that has been illuminated for one minute directly with the laser that drives the HHG source. The laser is focused to approximately 100 μm and reaches a fluence of 0.2 J/cm^2

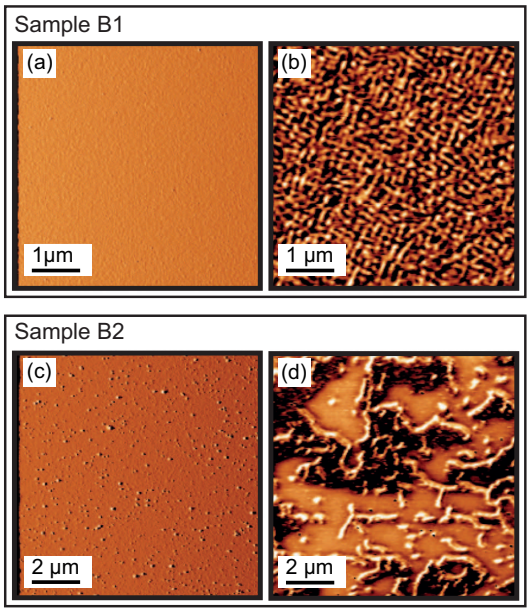

Fig. 2: (Colour on-line) Tapping-mode AFM (topography) and MFM (phase contrast at 30 nm lift of the magnetic tip) images of the as-grown sample (B1) are shown in (a) and (b). The corresponding images for the laser-illuminated sample (B2) are presented in (c) and (d). The AFM and MFM pictures have been taken on the frame of the particular sample next to the transparent membrane window at the same position.

per pulse at the sample. As we discuss in the following, the laser illumination of sample B2 results in several pronounced effects. First, the AFM image demonstrates that laser-ablated material re-deposits onto the sample surface in the form of nanometer-sized droplets (fig. 2(c)) [29–31]. Please note that the used laser fluence is close to the threshold of laser ablation, as it has been reported for other materials. However, accumulation effects due to repeated heating may contribute to the observed structural changes [32]. Furthermore, the domain structure has been modified (fig. 2(d)), resulting in a mixture of large ($\approx 1\,\mu$m) and small domains (≈ 100 nm). Moreover, three different contrast levels appear in the MFM image, suggesting the formation of a more complex magnetization pattern due to the canted easy axis of the film. However, the highly non-equilibrium transient state of the sample during laser exposure, resulting in the observed MFM image, is not yet understood. Note that figs. 2(c) and (d) have been measured on the sample frame next to the membrane window, supporting the heat dissipation, so that the sample degeneration is reduced compared to the window region. This position is marked with a black cross in an optical microscope image (fig. 3(a)), which shows as well laser-induced membrane wrinkling and a permanent laser imprint. The energy density profiles of the impinging laser light, shown in fig. 3(b), have been measured by placing the CCD detector at the sample plane.

Recently, it has been demonstrated that irreversible modifications of the magnetic anisotropy can be created

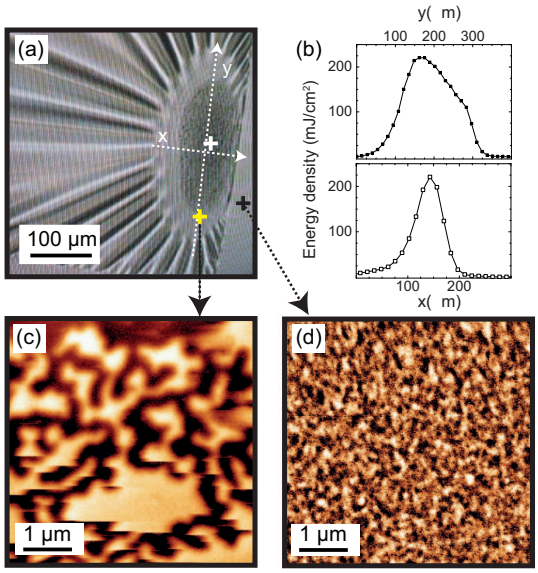

Fig. 3: (Colour on-line) (a) Optical micrograph of the laser-exposed sample B2. At the right edge of the image the rigid frame of the sample is visible. Energy density profiles along the white dashed lines are given in (b). After the film was saturated in an external out-of-plane field, MFM images were taken in remanence at the marked positions. At the center of the laser imprint (white cross) no magnetic structure has been detected, while the MFM images recorded at fringe of the imprint and at the solid frame (yellow and black crosses) are shown in (c) and (d), respectively.

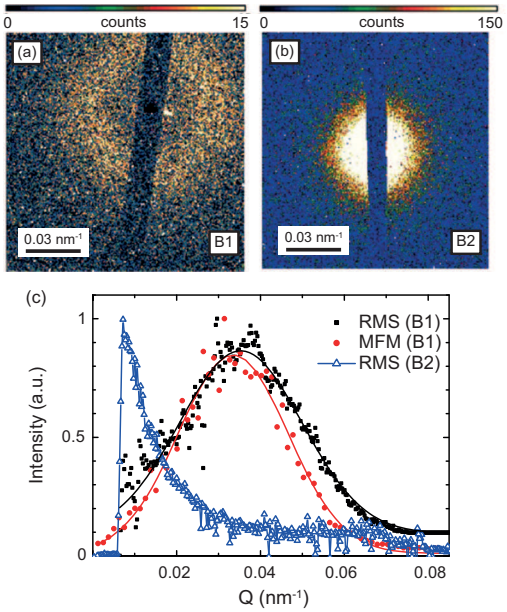

Fig. 4: (Colour on-line) RMS images from Co/Pt multilayers at the Co $M_{2,3}$-absorption edge for the as-grown sample B1 (a) and for the laser-exposed sample B2 (b). Radially integrated RMS signals in (c) are normalized to their maximum intensities. The black squares and blue triangles are the data points from B1 and B2, respectively. The red dots are taken from the radial integration of the squared Fourier transform of the MFM image from sample B1 (fig. 2(b)), and the black and red lines are Gaussian fits.

by femtosecond laser pulses of comparable energy densities [33]. In order to study the reversibility of the observed laser-induced modifications, sample B2 was saturated in an out-of-plane oriented magnetic field of 300 mT and again inspected at zero field with MFM. At the center of the laser imprint (at the white cross in fig. 3(a)) no magnetic contrast is detected. At the fringe of the imprint (yellow cross) we find a worm-like domain pattern with domain sizes of about 300 nm (fig. 3(c)).

The larger domain size indicates a permanent laser-induced enhancement of perpendicular magnetic anisotropy, an effect that has already been observed in ref. [33]. On the frame of the sample (black cross) a domain pattern with a domain size of approximately 100 nm is observed (fig. 3(d)), which is similar to the domain size of the as-grown sample B1. The MFM images demonstrate that the intense laser illumination has a permanent fluence-dependent impact on the magnetic domain structure that may be caused by laser sputtering, alloying, melting or interdiffusion (figs. 2(b) and (c)). Remarkably, the magnetic field can revert the laser-induced changes in the magnetic structure (fig. 2(d)), observed next to the visible laser imprint, and recreate a domain pattern similar to the as-grown state (fig. 3(d)). Studying ultrafast demagnetization with laser intensities close to the sample ablation threshold can potentially elucidate which dynamical processes lead to the formation of the complex domain pattern shown in fig. 2(d). Our RMS measurements of the two samples, which are presented below, demonstrate the feasibility of studying these processes by employing tabletop HHG beams.

The RMS images of the samples B1 and B2, integrated over an exposure time of 30 min, are shown in figs. 4(a) and (b). The signal-to-noise ratio has been enhanced by subtracting a dark image. For the RMS data from sample B1 we have applied a median filter over three neighboring pixels. Comparing these two measurements, it is apparent that the scattering patterns differ substantially. As shown in fig. 4(a), sample B1 scatters the XUV light into a ring, while sample B2 scatters the photons into a filled circle with a much smaller diameter (fig. 4(b)). The RMS pattern from sample B2 was measured directly after the laser illumination and the scattering pattern is independent of the beam position of the XUV probe spot on the 500 μm wide window, indicating a homogenous distribution of the scattering centers over the membrane. The radially integrated intensity derived from the RMS images is plotted in fig. 4(c). For a better comparison, both curves are normalized to their maximum intensity. The momentum transfer vector, Q, is calculated by $Q = \frac{4\pi}{\lambda}\sin(\frac{1}{2}\arctan(\frac{r}{D}))$, where λ denotes the wavelength, r is the radial distance to the directly transmitted beam in the scattering image and D is the distance between the camera and the sample, in this case 7 cm. The momentum transfer vector is

defined by $Q = 2\pi/d$, where d denotes the average distance between the scattering centers, *i.e.*, the domain periodicity for a magnetic structure. For sample B1 (black curve) the radially integrated signal exhibits a peak centered at $0.035\,\mathrm{nm}^{-1}$, corresponding to an average periodicity of 180 nm. Assuming the same size for the antiparallel oriented domains, this implies an average width of the domains of about 90 nm. This result matches very well with the average domain size of 92 nm extracted from the radial integration of the squared magnitude of the Fourier transformed MFM image, which displays a peak at $0.034\,\mathrm{nm}^{-1}$ (red curve). The peak position has been determined using Gaussian fits, yielding similar values of the FWHM for the RMS ($0.034\,\mathrm{nm}^{-1}$) and the MFM ($0.031\,\mathrm{nm}^{-1}$) data. Taking into account the measurement uncertainty in the lateral resolution of the MFM (*e.g.*, due to the fringing fields between MFM-tip and the sample surface) and the spectral bandwidth of the HHG source, RMS and MFM measurements are in very good agreement regarding the average domain size and the corresponding size distribution.

The MFM image of sample B2 taken after the laser exposure (but before applying an external field) exhibits much larger domains compared to B1 (fig. 2), which is expected to result in smaller momentum transfer vectors, in case similar magnetic structures are also created within the membrane window. The scattering curve indeed reveals that a large part of the scattered light is distributed close to the 0th diffraction order (blue curve). The intensity maximum is apparently hidden underneath the beam block, *i.e.*, it is located at a Q value smaller than $0.008\,\mathrm{nm}^{-1}$, implying that the average distance between the scattering centers is larger than 785 nm. We note that the XUV flux before the sample reaches 3×10^7 photons per second and the ratio of scattered to incoming photons is estimated by 2×10^{-5} and 2.1×10^{-4} for B1 and B2, respectively. Consequently, for sample B2, the scattering probability is one order of magnitude larger compared to sample B1, which hints at a different origin of the observed scattering pattern.

To identify the scattering source, the RMS measurement of sample B2 was repeated in an out-of-plane magnetic field of 300 mT, introducing a single-domain state. Nevertheless, the scattering image was identical to the signal detected before applying the external field. The latter observation excludes the possibility that the scattering pattern is of magnetic origin. On the other hand, the AFM image (fig. 2(c)) suggests that the generated droplets, which modify the morphology of the specimen, are responsible for the observed increase of the scattering intensity, as well as for the change in the radial distribution. The average distance between these droplets is on the micrometer scale, which agrees with the lower limit approximation of 785 nm, measured with the XUV-light scattering experiment. Our results show that pump-probe investigations of the temporal evolution of the domain pattern with intense pump pulses will require a precise tuning of the laser power to avoid the generation of such non-magnetic scattering effects.

In summary, we have analyzed the magnetic structure and morphology in Co/Pt multilayer films employing AFM, MFM and resonant magnetic scattering (RMS). We found that the XUV light generated by 2 mJ laser pulses can be successfully applied for the characterization of a randomly arranged predominantly out-of-plane domain pattern on the scale below 100 nm. We ascribe the observed scattering patterns to the magnetic structure as well as to morphology changes, caused by the exposure with ultrashort infrared laser pulses, reaching a fluence of $0.2\,\mathrm{J/cm}^2$. Our MFM analysis shows that magnetic modifications are partially reversible. Nevertheless, the permanent morphology changes contribute substantially and must be taken into account in interpretation of the scattering images.

* * *

The authors thank the Deutsche Forschungsgemeinschaft for funding under the project SCHN 353/17 and L. Müller (DESY) for valuable discussions. The JILA group gratefully acknowledges funding from the U.S. Department of Energy Office of Basic Energy Sciences, Award No. DE-SC0002002, the Deutsche Forschungsgemeinschaft No. GR 4234/1-1, and from the Physics Frontiers Center Program. The Hamburg group acknowledges support from "The Hamburg Centre for Ultrafast Imaging".

REFERENCES

[1] Stamm C., Kachel T., Pontius N., Mitzner R., Quast T., Holldack K., Khan S., Lupulescu C., Aziz E. F., Wietstruk M., Dürr H. A. and Eberhardt W., *Nat. Mater.*, **6** (2007) 740.

[2] Radu I., Vahaplar K., Stamm C., Kachel T., Pontius N., Dürr H. A., Ostler T. A., Barker J., Evans R. F. L., Chantrell R. W., Tsukamoto A., Itoh A., Kirilyuk A., Rasing Th. and Kimel A. V., *Nature*, **472** (2011) 205.

[3] Pfau B., Schaffert S., Müller L., Gutt C., Al-Shemmary A., Büttner F., Delaunay R., Düsterer S., Flewett S., Frömter R., Geilhufe J., Guehrs E., Günther C. M., Hawaldar R., Hille M., Jaouen N., Kobs A., Li K., Mohanty J., Redlin H., Schlotter W. F., Stickler D., Treusch R., Vodungbo B., Kläui M., Oepen H. P., Lüning J., Grübel G. and Eisebitt S., *Nat. Commun.*, **3** (2012) 1100.

[4] La-O-Vorakiat C., Siemens M., Murnane M. M., Kapteyn H. C., Mathias S., Aeschlimann M., Grychtol P., Adam R., Schneider C. M., Shaw J. M., Nembach H., Silva T. J., *Phys. Rev. Lett.*, **103** (2009) 257402.

[5] Mathias S., La-O-Vorakiat C., Grychtol P., Granitzka P., Turgut E., Shaw J. M., Adam R., Nembach H. T., Siemens M. E., Eich S., Schneider

C. M., Silva T. J., Aeschlimann M., Murnane M. M. and Kapteyn H. C., *Proc. Natl. Acad. Sci. U.S.A.*, **109** (2012) 4792.

[6] Rudolf D., La-O-Vorakiat C., Battiato M., Adam R., Shaw J. M., Turgut E., Maldonado P., Mathias S., Grychtol P., Nembach H. T., Silva T. J., Aeschlimann M., Kapteyn H. C., Murnane M. M., Schneider C. M. and Oppeneer P. M., *Nat. Commun.*, **3** (2012) 1037.

[7] Turgut E., La-O-Vorakiat C., Shaw J. M., Grychtol P., Nembach H. T., Rudolf D., Adam R., Aeschlimann M., Schneider C. M., Silva T. J., Murnane M. M., Kapteyn H. C. and Mathias S., *Phys. Rev. Lett.*, **110** (2013) 197201.

[8] Vodungbo B., Gautier J., Lambert G., Barszczak Sardinha A., Lozano M., Sebban S., Ducousso M., Boutu W., Li K., Tudu B., Tortarolo M., Hawaldar R., Delaunay R., López-Flores V., Arabski J., Boeglin C., Merdji H., Zeitoun P. and Lüning, J., *Nat. Commun.*, **3** (2012) 999.

[9] Li J., Lee M., He W., Redeker B., Remhof A., Amaladass E., Hassel C. and Eimüller T., *Rev. Sci. Instrum.*, **80** (2009) 073703.

[10] Graves C. E., Reid A. H., Wang T., Wu B., de Jong S., Vahaplar K., Radu I., Bernstein D. P., Messerschmidt M., Müller L., Coffee R., Bionta M., Epp S. W., Hartmann R., Kimmel N., Hauser G., Hartmann A. *et al.*, *Nat. Mater.*, **12** (2013) 293.

[11] Popmintchev T., Chen M., Popmintchev D., Arpin P., Brown S., Alisauskas S., Andriukaitis G., Balciunas T., Mücke O. D., Pugzlys A., Baltuska A., Shim B., Schrauth S. E., Gaeta A., Hernández-García C., Plaja L., Becker A., Jaron-Becker A., Murnane M. M. and Kapteyn H. C., *Science*, **336** (2012) 1287.

[12] Kfir O., Grychtol P., Turgut E., Knut R., Zusin D., Popmintchev D., Popmintchev T., Nembach H., Shaw J., Fleischer A., Kapteyn H., Murnane M. and Cohen O., arXiv e-print, arXiv:1401.4101.

[13] Wieland M., Spielmann Ch., Kleineberg U., Westerwalbesloh Th., Heinzmann U. and Wilhein T., *Ultramicroscopy*, **102** (2005) 93.

[14] Seaberg M. D., Adams D. E., Townsend E. L., Raymondson D. A., Schlotter W. F., Liu Y., Menoni C. S., Rong L., Chen C., Miao J., Kapteyn H. C. and Murnane M. M., *Opt. Express*, **19** (2011) 22470.

[15] Zhang B., Seaberg M. D., Adams D. E., Gardner D. F., Shanblatt E. R., Shaw J. M., Chao W., Gullikson E. M., Salmassi F., Kapteyn H. C. and Murnane M. M., *Opt. Express*, **21** (2013) 21970.

[16] Hillebrecht F. U., Kinoshita T., Spanke D., Dresselhaus J., Roth Ch., Rose H. B. and Kisker E., *Phys. Rev. Lett.*, **75** (1995) 2224.

[17] Grychtol P., Adam R., Valencia S., Cramm S., Bürgler D. E. and Schneider C. M., *Phys. Rev. B*, **82** (2010) 054433.

[18] Hannon J. P., Trammell G. T., Blume M. and Gibbs D., *Phys. Rev. Lett.*, **61** (1988) 1245.

[19] Eisebitt S., Lörgen M., Eberhardt W., Lüning J. and Stöhr J., *Appl. Phys. A*, **80** (2005) 921.

[20] Gutt C., Streit-Nierobisch S., Stadler L.-M., Pfau B., Günther C. M., Könnecke R., Frömter R., Kobs A., Stickler D., Oepen H. P., Fäustlin R. R., Treusch R., Feldhaus J., Weckert E., Vartanyants I. A. *et al.*, *Phys. Rev. B*, **81** (2010) 100401(R).

[21] Kapteyn H. C., Murnane M. M. and Christov I. P., *Phys. Today*, **58**, issue No. 3 (2005) 39.

[22] Ge X., Ducousso M., Boutu W., Tudu B., Barbrel B., Gauthier D., Borta A., Gonzalez A.-I., Wang F., Iwan B., Billon M., Perdrix M., Guillaumet D., Lepetit F., Vodungbo B., Gautier J., Hawaldar R., Tortarolo M., Delaunay R., Zeitoun P., Lüning J., and Merdji H., *J. Mod. Opt.*, **60** (2013) 1475.

[23] Frömter R., Stillrich H., Menk C. and Oepen H. P., *Phys. Rev. Lett.*, **100** (2008) 207202.

[24] Hille M., Frauen A., Beyersdorff B., Kobs A., Hesse S., Frömter R. and Oepen H. P., *J. Appl. Phys.*, **113** (2013) 023902.

[25] Stickler D., Frömter R., Stillrich H., Menk C., Oepen H. P., Gutt C., Streit-Nierobisch S., Stadler L.-M., Grübel G., Tieg C. and Yakhou-Harris F., *Phys. Rev. B*, **84** (2011) 104412.

[26] Streit-Nierobisch S., Stickler D., Gutt C., Stadler L.-M., Stillrich H., Menk C., Frömter R., Tieg C., Leupold O., Oepen H. P. and Grübel G., *J. Appl. Phys.*, **106** (2009) 083909.

[27] Wang T., Zhu D., Wu B., Graves C., Schaffert S., Rander T., Müller L., Vodungbo B., Baumier C., Bernstein D. P., Bräuer B., Cros V., de Jong S., Delaunay R., Fognini A., Kukreja R., Lee S., López-Flores V., Mohanty J., Pfau B., Popescu H., Sacchi M., Sardinha A. B., Sirotti F., Zeitoun P., Messerschmidt M., Turner J. J., Schlotter W. F., Hellwig O., Mattana R., Jaouen N., Fortuna F., Acremann Y., Gutt C., Dürr H. A. *et al.*, *Phys. Rev. Lett.*, **108** (2012) 267403.

[28] Müller L., Gutt C., Pfau B., Schaffert S., Geilhufe J., Büttner F., Mohanty J., Flewett S., Treusch R., Düsterer S., Redlin H., Al-Shemmary A., Hille M., Kobs A., Frömter R., Oepen H. P., Ziaja B., Medvedev N., Son S-K., Thiele R., Santra R., Vodungbo B., Lüning J., Eisebitt S. and Grübel G., *Phys. Rev. Lett.*, **110** (2013) 234801.

[29] Leitz K-H., Redlingshfer B., Reg Y., Otto A. and Schmidt M., *Phys. Proc.*, **12B** (2011) 230.

[30] Siew W. O., Lee W. K., Wong H. Y., Yong T. K., Yap S. S. and Tou T. Y., *Appl. Phys. A*, **101** (2010) 627.

[31] Andreić Ž., Aschke L. and Kunze H.-J., *Appl. Surf. Sci.*, **153** (2000) 235.

[32] Mannion P. T., Magee J., Coyne E., O'Connor G. M. and Glynn T. J., *Appl. Surf. Sci.*, **233** (2004) 275.

[33] Kisielewski J., Dobrogowski W., Kurant Z., Stupakiewicz A., Tekielak M., Kirilyuk A., Kimel A., Rasing Th., Baczewski L. T., Wawro A., Balin K., Szade J. and Maziewski A., *J. Appl. Phys.*, **115** (2014) 053906.